RADIO SCIENCE, VOL. 45, RS2003, doi:10.1029/2009RS004169, 2010

X band model of Venus atmosphere permittivity

Xueyang Duan,[1] Mahta Moghaddam,[1] Daniel Wenkert,[2] Rolando L. Jordan,[2] and Suzanne E. Smrekar[2]

Received 5 March 2009; revised 3 November 2009; accepted 18 November 2009; published 2 April 2010.

[1] A model of Venus' atmosphere permittivity profile up to 300 km is developed in this paper for X band. The model includes both the real and imaginary parts of the atmospheric permittivity, derived using data sets inferred or directly measured from past exploration missions to Venus: the real part is obtained by calculating the total polarization of the mixture of the atmospheric components including CO_2, N_2, H_2O, SO_2, H_2SO_4, CO, etc.; the imaginary part is derived using the superposition of the absorption of each component. The properties of the atmospheric components such as polarization and absorption are modeled with respect to frequency, temperature, and pressure. The validity of this model is verified by comparing simulation results with available measurements of Venus' atmosphere. This permittivity model is intended as a critical tool for the design of next-generation orbiting radar systems, in particular interferometric radars.

Citation: Duan, X., M. Moghaddam, D. Wenkert, R. L. Jordan, and S. E. Smrekar (2010), X band model of Venus atmosphere permittivity, *Radio Sci.*, *45*, RS2003, doi:10.1029/2009RS004169.

1. Introduction

[2] During the past 30 years, several satellite missions have been carried out to study the surface of Venus. In particular, orbiting radars have been utilized to study the Venus surface structure dating back to the American Pioneer Venus project (1978 to 1992). Although at low resolution (~5–20 km), the Magellan mission (1990 to 1994) provided the best global altimetry for Venus to date. These topographic data were important for understanding the basic physiography of Venus and identifying its important surface features. In addition, stereo topography data for parts of Venus (>17% of the planet) were generated using radar images obtained at different look angles. This stereo data set, which provides almost 100 times better horizontal resolution (~100 m) than the altimeter [*Ford et al.*, 1993], has been immensely important for addressing more detailed geologic questions, particularly those related to tectonic structures, resurfacing, and stratigraphy.

[3] Nevertheless, the existing stereo data on Venus can only be used to study a small range of questions over a small fraction of the planet; also, the stereo data have only limited relative vertical precision (~10 m) [*Howington-Kraus et al.*, 2001]. Analogous to the information revealed from the Mars' high-resolution topography provided by Mars Orbiter Laser Altimeter (MOLA), fundamental questions in the study of Venus, such as how resurfacing of the planet occurred within the last 1 Gy and why geologic activity may have declined following the resurfacing [*Phillips et al.*, 1992; *Phillips and Izenberg*, 1995], are expected to be addressed with high-resolution topography of Venus. Hence, there has been significant recent interest in investigating radar systems for measuring Venus' topography with high resolution. In particular, the feasibility of X band altimeter and/or SAR interferometer systems are being examined.

[4] To design this system, the effects of the Venusian atmosphere on an X band signal must first be estimated. However, in past and current Venus missions, no synthesized information on the atmosphere's influence on electromagnetic wave propagation has been delivered. To address this need for the design of next-generation Venus radar missions, a model of Venus atmosphere permittivity as a function of altitude up to 300 km has been developed in this work. Moreover, although the focus of this work is on the X band model, it is noted that important measurements have also been made at S band [*Pettengill et al.*, 1996]. The reason for immediate emphasis on X band is that InSAR systems at X band are

[1]Department of Electrical Engineering and Computer Science, University of Michigan, Ann Arbor, Michigan, USA.
[2]Jet Propulsion Laboratory, Pasadena, California, USA.

0048-6604/10/2009RS004169

expected to be more efficient in mapping the Venus surface topography than other frequencies. Specially, they are more compact (smaller antenna and interferometric baseline), have higher resolution, and are less impacted by the ionosphere. Furthermore, the use of dual-frequency measurements can potentially lend to enhanced discoveries about the atmosphere and surface of Venus [*Jenkins et al.*, 1994]. Therefore, a similar atmospheric model at S band will be quite valuable as well and is a subject for future research. The methodology developed here for X band will be equally valid at S band if the input data are also available at S band frequency.

[5] To construct the Venus atmosphere permittivity model, many types of information are required, including temperature, pressure, material composition, properties of the ionosphere, and properties of the cloud layer. Past and current Venus missions provide significant information on these parameters. The temperature, pressure, and density profiles (up to 100 km) are mainly provided by the Venera, Pioneer Venus and VEGA missions [*Seiff et al.*, 1985; *Zasova et al.*, 2006]. The Venus Express Radio Science (VeRa) experiment gives the most recent temperature and pressure profiles with detailed analysis including variations with latitudes [*Tellmann et al.*, 2009]. The cloud properties (~40 km to 60 km) are based on the Pioneer Venus project observations [*Knollenberg and Hunten*, 1980; *James et al.*, 1997]. Information on Venusian atmospheric composition under the cloud is contributed by Magellan radio occultations [*Kolodner and Steffes*, 1998] and ground-based microwave observations [*Jenkins et al.*, 2002], in addition to the missions mentioned above [*de Bergh et al.*, 2006]. The gaseous mixing ratios in Venus' mesosphere were recently updated by results delivered from the Venus Express project [*Fedorova et al.*, 2008; *Vandaele et al.*, 2008], which also provides the most recent distribution of the ionosphere [*Pätzold et al.*, 2007].

[6] Venus' atmosphere consists mainly of carbon dioxide (slightly less than 96.5%) and nitrogen (slightly less than 3.5%). Trace gases include water vapor, sulfur compounds, and carbon monoxide. The planet's surface pressure can reach 90 atm, with surface temperature of around 700 K. Thick clouds consisting of sulfuric acid droplets exist at lower altitudes (~40 km to 60 km) in the Venus atmosphere. The high atmospheric density resulting from high pressure and temperatures considerably impacts on electromagnetic wave propagation. Also both the clouds and the atmospheric gases cause significant absorption of the radio signals [*Janssen and Poynter*, 1981; *Kolodner and Steffes*, 1998].

[7] To study the electromagnetic wave propagation characteristics through Venus' atmosphere, its complex permittivity profile must be known. The real part of the complex permittivity is used to find the propagation coefficient, and the imaginary part accounts for the signal absorption. Since the complex permittivity is frequency-dependent, to investigate the X band signal propagation for future radar mission design, Venus atmosphere permittivity at that frequency needs to be derived.

[8] In this work, a model was constructed for the real and the imaginary parts of the Venus atmosphere permittivity profile. Using the relationship between the permittivity and polarization of polar materials, the real part of the atmospheric permittivity was obtained by calculating the total polarization of the mixture of known components. The contribution of each component was calculated based on the assumed known (though arbitrary) component fraction in the mixture. For each atmospheric component, its polarization was modeled as a function of frequency, temperature, and pressure based on the available information in the literature. The imaginary part of the atmospheric permittivity was found from the available measurements of the mixture component absorptions. The temperature and pressure dependences of the absorption from each component were modeled using the data and information given in the literature. The model was verified by comparing the simulation results with those inferred from the absorption and the refractivity data acquired from previous missions to Venus and from ground-based measurements.

[9] This article is organized as follows: Section 2 describes the construction of the permittivity model, including the real and the imaginary parts. Section 3 presents the simulation results and the model verification based on the available Venus observation data. Finally, section 4 concludes the article with a discussion of possible improvements to the model in the future. Application of this permittivity model in studying the X band signal propagation for a future radar mission is being reported in a separate paper by the authors.

2. Model Construction

[10] The Venus atmosphere permittivity model is constructed for both the real and the imaginary parts. In this work, the dielectric constant is used to refer to the real part of the relative permittivity. The dielectric constant ϵ_r' is found by calculating the total polarization of the mixture of known atmospheric components; the imaginary part of the relative atmospheric permittivity ϵ_r'' is obtained using the measured absorptions of the mixture components. The total complex relative permittivity is given by

$$\epsilon_r = \epsilon_r' + i\epsilon_r'' \tag{1}$$

and the total complex permittivity is $\epsilon = \epsilon_r\epsilon_0$, where $\epsilon_0 = 8.854 \times 10^{-12}$ F/m is the permittivity of free space.

2.1. Dielectric Constant of the Venus Atmosphere

[11] The dielectric constant ϵ_r' is modeled utilizing its relation with the total polarization of the atmospheric mixture. To get the polarization of the mixture, the approach of *Harvey and Prausnitz* [1987] and *Harvey and Lemmon* [2005] is applied. Using this method, the polarization of each atmospheric component is added into the total polarization of the atmospheric mixture maintaining the component density. Though this method was developed for calculating the static dielectric constant of a fluid mixture in the work of *Harvey and Lemmon* [2005], for the dielectric constant value at X band, the mixing principle is still valid as long as the corresponding X band dielectric constant values and polarizations are used.

2.1.1. Relation Between Polarization and Dielectric Constant

[12] Polarization or polarization density is the density of permanent or induced electric dipole moments in a dielectric material. It is directly related to the material dielectric constant. The relationship between polarization and dielectric constant is different for polar and nonpolar materials, both of which exist in the Venusian atmosphere. For example, CO_2 and N_2 are nonpolar molecules, while H_2O and SO_2 are polar molecules.

[13] There are three mechanisms producing electric polarization for dielectrics [*Boettcher*, 1973]: (1) dipole or orientational polarization, which exists in polar media possessing permanent dipole moments, (2) ionic or molecular polarization, existing in materials including positive and negative ions that tend to displace themselves when an electric field is applied, and (3) electronic polarization, which exists in most materials; the applied electric field displaces the electric cloud center of an atom relative to the center of the nucleus. For nonpolar gases, only the electronic polarization needs to be considered while in the polar gases, both the orientational polarization and the electronic polarization are important.

[14] As described by *Kirkwood* [1936], the electric dipole moment in a nonpolar material is proportional to the field acting on the molecule; this dependence is defined as polarizability α_T. The electric dipole moment is $p = \alpha_T \frac{F}{E}$, where E is the applied electric field amplitude, and F is the average local field in the interior of the molecule. With microscopic modeling of molecular moment and macroscopic relation between polarization and the applied field [*Kirkwood*, 1936], the Clausius-Mosotti formula can be deduced to describe the relation between polarization and dielectric constant for a nonpolar material,

$$\frac{P_0}{v} = \frac{\epsilon_r' - 1}{\epsilon_r' + 2} \tag{2}$$

where v is the molar volume and P_0 is the molecular polarization, which has the units of volume.

[15] For a polar material, both the orientational polarization and the electronic polarization must be considered in the electric dipole moment $p = \mu + \alpha_T \frac{F}{E}$ [*Kirkwood*, 1939], where μ accounts for the effect of the permanent dipole moment that produces the orientational polarization. The second term describes the electronic polarization as mentioned above. With different microscopic modeling and similar macroscopic relation as in the nonpolar case [*Kirkwood*, 1939], the following expression can be used to relate polarization and dielectric constant ϵ_r' in the polar material:

$$\frac{P_0}{v} = \frac{\left(\epsilon_r' - 1\right)\left(2\epsilon_r' + 1\right)}{9\epsilon_r'} \tag{3}$$

Equations (2) and (3) apply for general fluids, including liquids and gases.

[16] Since the Venusian atmosphere is a mixture of both polar and nonpolar molecules, its dielectric constant can be treated similarly to the polar material case in that both the orientational polarization and the electronic polarization have to be considered. With a low fraction of the polar gases, the term μ, which accounts for the orientational polarization, would be small; however, this does not affect the macroscopic relation described by the Kirkwood model, which can be applied for the mixture of polar and nonpolar fluids.

[17] When the applied electric field is time-dependent, polarization and dielectric constant are both functions of frequency. Compared to the static case, the polarization need not be in equilibrium in a dynamic field, since motions of microscopic particles require a certain time to reach a certain polarization value; the amount of time required is the characteristic time of the material. However, due to the low density of its fluid phase, Venus' atmosphere can be treated as being quasi-static in the microwave region. Therefore, the derivations of above relations using the statistical-mechanical theories in the equilibrium case still hold [*Boettcher*, 1973], indicating that the relationships between polarization and dielectric constant shown in equations (2) and (3) are admissible for the X band analysis.

2.1.2. Polarization of Fluid Mixture

[18] The contribution of each atmospheric component to the polarization of the mixture can be calculated under a given temperature and with its reduced density, which is described in detail below. This method maintains the density of the component in the mixture when calculating the polarization of the pure material. As shown by *Harvey and Prausnitz* [1987], the total polarization of a mixture can be written as:

$$P_{mix} = \sum_i \Phi_i^* P_i\left(T, \frac{\rho_{r,mix}}{v_i^*}\right) \tag{4}$$

where v_i^* is a characteristic molar volume for component i. It can be the critical volume of the gas (the volume of one mole substance measured at its critical temperature and pressure) or its characteristic volume under known conditions (temperature, pressure, etc.). $\frac{\rho_{r,mix}}{v_i^*}$ is the reduced density of the ith component. The quantity $\rho_{r,mix}$ is dimensionless and defined as:

$$\rho_{r,mix} = \rho_{mix} \sum_i x_i v_i^* \tag{5}$$

The volume fraction Φ_i^* is defined using the characteristic volumes as:

$$\Phi_i^* = \frac{x_i v_i^*}{\sum_j x_j v_j^*} \tag{6}$$

where x_i is the molar fraction of ith component.

[19] Given the values of temperature and pressure, the reduced density acts as the ratio of total 'reduced' volume of the mixture, which is obtained from the characteristic volume and the molar fraction of each component, to the real volume of the mixture. The polarization of each atmospheric component, which is $P_i\left(T, \frac{\rho_{r,mix}}{v_i^*}\right)$ in equation (4), is evaluated under the condition corresponding to its characteristic volume. The polarization densities of all components are then added up to obtain the polarization of the total mixture for the given temperature and pressure.

[20] To find the mixture polarization using equation (4), the polarization of the ith component is required at the same temperature as the mixture and with the reduced density $\frac{\rho_{r,mix}}{v_i^*}$. Therefore, polarization of each component in the Venus atmosphere and its dependence on temperature and density, or pressure, need to be investigated.

2.1.3. Polarization of the Nonpolar Venus Atmospheric Components

[21] As discussed by *Harvey and Lemmon* [2005], ratio of polarization to the molar density ρ can be expanded in a power series known as the dielectric virial expansion:

$$\frac{P}{\rho} = A_\epsilon + B_\epsilon \rho + C_\epsilon \rho^2 + \cdots \tag{7}$$

The first dielectric virial coefficient A_ϵ is proportional to the molecular polarizability and slightly dependent on the temperature. The molecular rotational effect, which is most important to the molecules and the temperature range of interest here, gives an approximately linear increase of A_ϵ with temperature [*Harvey and Lemmon*, 2005].

[22] The second dielectric virial coefficient B_ϵ describes the interactions between pairs of molecules. It is approximately linear with $\frac{1}{T}$ for a nonpolar material. Based on the analysis of *Harvey and Lemmon* [2005], both A_ϵ and B_ϵ can be extracted from the measured laboratory data.

[23] According to *Harvey and Lemmon* [2005], dielectric virial coefficient C_ϵ is less important for gas-phase fluids. Due to the difficulty of extracting higher-order terms from their laboratory data, an empirical term $C\rho^D$ is chosen for extending the correlation to high densities as follows:

$$\frac{P}{\rho} = A_\epsilon + B_\epsilon \rho + C\rho^D \tag{8}$$

Dependences of these dielectric virial coefficients on temperature are given by:

$$A_\epsilon = a_0 + a_1\left(\frac{T}{T_0} - 1\right) \tag{9}$$

$$B_\epsilon = b_0 + b_1\left(\frac{T_0}{T} - 1\right) \tag{10}$$

$$C = c_0 + c_1\left(\frac{T_0}{T} - 1\right) \tag{11}$$

where T_0 is 273.16 K; T is the temperature in Kelvin.

[24] For CO_2 and N_2, the parameters in above equations are taken from *Harvey and Lemmon* [2005] and given in Table 1. These values are for the polarization in a static field. However, as shown by *Boettcher* [1978], dispersion of the dielectric constant with respect to frequency is determined by locations of the absorption frequencies and expansion of the absorption line of the molecules. For nonpolar materials, rotational absorption, which accounts for the absorption at the microwave region, is not important. Hence, the nonpolar materials have absorption frequencies much higher than X band. For example, the first absorption frequencies of CO_2 are in the wavelength range of several microns. Therefore, the coefficient values for the static case given in Table 1 are expected to be valid in X band.

[25] The volume fractions of the two major gases, CO_2 and N_2, are widely accepted to be approximately 96.5% and 3.5%, respectively [*de Bergh et al.*, 2006]. Considering both of them as ideal gases (equation of state: $pV = nRT$; p is pressure in atm, V is volume in m^3, n is the number of moles, R is the gas constant

Table 1. Parameters for Mixture Components[a]

Fluid	a_0	a_1	b_0	b_1	c_0	c_1	D
CO_2	7.3455	0.00335	83.93	145.1	−578.8	−1012.	1.55
N_2	4.3872	0.00226	2.206	1.135	−169.0	−35.83	2.1
Ar	4.1414	0	1.597	0.262	−117.9	0	2.1
He	0.517254	0	−0.203	0.039	7.47	0	2
Ne	0.9969	0	−0.109	0.0708	−2.88	−1.0	2

[a]Source: *Harvey and Lemmon* [2005].

82.057 $cm^3 \cdot atm \cdot K^{-1}\ mol^{-1}$ and T is the absolute temperature), the volume fractions can be directly used as the molar fractions in the mixing formula. For more accurate calculations, the van der Waals equation can be utilized as the equation of state,

$$\left(p + \frac{n^2 a}{V^2}\right)(V - nb) = nRT \tag{12}$$

where a and b are van der Waals constants; $a = 3.592 \times 10^6\ cm^6 \cdot atm/mol^2$, $b = 0.04267 \times 10^3\ cm^3/mol$ for CO_2; $a = 1.390 \times 10^6\ cm^6 \cdot atm/mol^2$, $b = 0.03913 \times 10^3\ cm^3/mol$ for N_2.

2.1.4. Polarization of the Polar Venus Atmospheric Components

[26] Most trace gases in the Venusian atmosphere are polar molecules, such as H_2O, SO_2, H_2SO_4, CO, etc. For the polar molecules, the rotational absorption extends their absorption spectrum to the microwave region. These low-frequency absorption lines and the pressure broadening play important roles in determining the dispersion of polarization with frequency in X band. Therefore, though the total amount of these minor constituents make up less than 1% volume fraction in the atmosphere, their effects on the atmospheric permittivity are examined and included in this model.

2.1.4.1. Water Vapor

[27] To include the polarization of water vapor (H_2O) into the atmosphere mixture, its value at X band as a function of temperature and density needs to be investigated. The first absorption frequency of water which may have an effect is a weak line at 22.235 GHz. However, due to the low density of the water vapor, broadening of this line is very limited with little effect in X band. Therefore, the dispersion of water vapor is negligible at this frequency, which is proven by the lab measurements of *Birnbaum* [1952]. However, since the surface temperature on Venus is as high as 700 K, the *Birnbaum* [1952] model (measured at 9.28 GHz and verified from 24.5°C to 103°C) may not be accurate. Therefore, another two models describing more accurately the behavior of the water vapor dielectric constant as a function of temperature and pressure were considered. One is the measurement data-fitted model by *Uematsu and Franck* [1980] (temperature: 0 to 823.15 K, pressure: up to 4935 atm), which is given by

$$\begin{aligned}\epsilon_r' = 1 &+ \left(\frac{A_1}{T^*}\right)\rho^* + \left(\frac{A_2}{T^*} + A_3 + A_4 T^*\right)\rho^{*2} \\ &+ \left(\frac{A_5}{T^*} + A_6 T^* + A_7 T^{*2}\right)\rho^{*3} \\ &+ \left(\frac{A_8}{T^{*2}} + \frac{A_9}{T^*} + A_{10}\right)\rho^{*4}\end{aligned} \tag{13}$$

where $\rho^* = \rho/\rho_0$, $T^* = T/T_0$, ρ is density in kg/m^3 and T is temperature in Kelvin. Coefficients of equation (13) are listed in Table 2.

[28] The other model given by *Pitzer* [1983] is in analytic form and more easily extrapolated to higher temperatures (3% error at 850 K). In this model, the polarization per molar volume P_v is given by

$$P_v = \frac{(\epsilon_r' - 1)(2\epsilon_r' + 1)}{9\epsilon_r'} = \frac{4\pi N_0 d}{3M}\left(\alpha_T + \frac{\mu^2 g}{3kT}\right) \tag{14}$$

where the Kirkwood correlation factor $g = 1 + 2.68d + 6.69d^5\left[\left(\frac{565}{T}\right)^{0.3} - 1\right]$. It accounts for the nonrandom orientation of neighboring molecules and can be approximated as 1 for the gas phase, indicating a linear relation between density and polarization [*Boettcher*, 1973]. N_0 in equation (14) is the Avogadro's number which is the number of particles in one mole, $N_0 = 6.023 \times 10^{23}\ mol^{-1}$; d is the density in g/cm^3, M is the molecular weight in g/mol, k is the Boltzmann constant. α_T and μ are the molecular polarizability and the molecular dipole moment having the values $1.444 \times 10^{-24}\ cm^{-3}$ and 1.84×10^{-18} esu · cm, respectively. The dielectric constant can be found from the polarization given by this model.

[29] The dielectric constant values resulting from the above two models agree with each other very well under the conditions of interest (differed less than 1% for density < 0.1 g/cm^3 and temperature from 150 K to 700 K).

Table 2. Coefficients for Equation (13)[a]

Coefficient	Value
A_1	7.62571×10^0
A_2	2.44003×10^2
A_3	-1.40569×10^2
A_4	2.77841×10^1
A_5	-9.62805×10^1
A_6	4.17909×10^1
A_7	-1.02099×10^1
A_8	-4.52059×10^1
A_9	8.46395×10^1
A_{10}	-3.58644×10^1
T_0	298.15 K
ρ_0	1000 kg/m^3

[a]Source: *Uematsu and Franck* [1980].

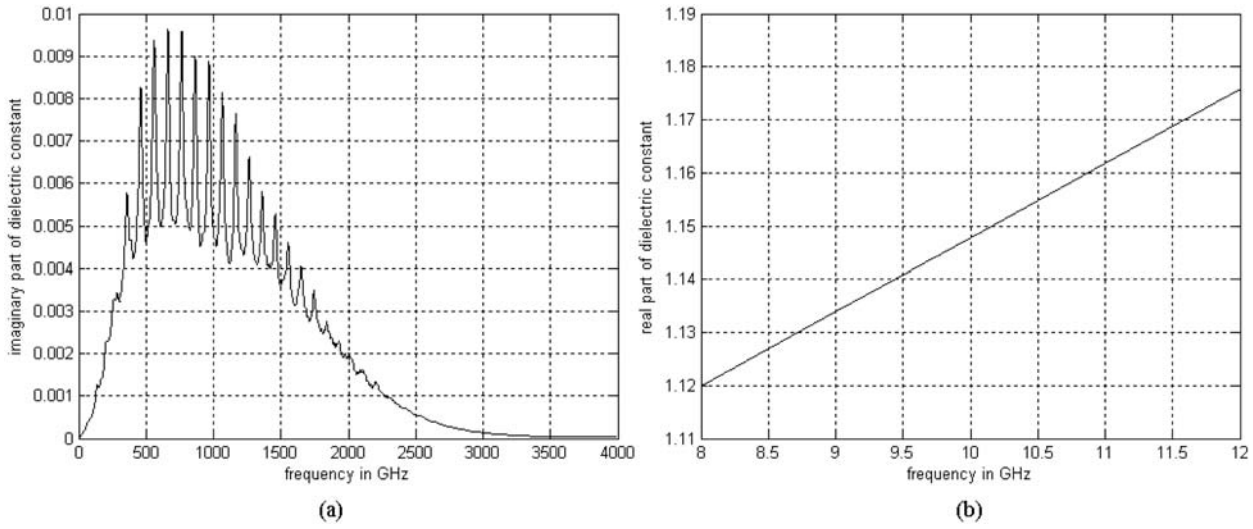

Figure 1. (a) Convergence check for SO_2: ϵ_r'' versus frequency; (b) ϵ_r' of SO_2 in X band. ($T = 0°C$, pressure is 1 atm.)

Considering the accuracy of the available temperature profile and extendibility to higher temperatures, the *Pitzer* [1983] model is utilized in this work. To apply the mixing rules of *Harvey and Lemmon* [2005], the characteristic molar volume of 18.80407 cm^3/mol is used for the water vapor given the pressure of 1 atm and the temperature of 100°C.

2.1.4.2. Sulfur Dioxide

[30] Sulfur dioxide (SO_2) has numerous absorption lines in the microwave region; hence dispersion is expected for this constituent. Due to the limited information available in the literature about the SO_2 dielectric constant in X band, the relation between the real and the imaginary parts of complex permittivity, known as the Kramers-Kroenig rule, is used here to obtain ϵ_r'. From the knowledge of the imaginary part of the permittivity ϵ_r'' over the whole frequency range, ϵ_r' can be calculated as:

$$\epsilon_r'(\omega) - \epsilon_{r\infty} = \frac{1}{\pi}\int_{-\infty}^{\infty} \frac{\epsilon_r''(\omega')}{\omega' - \omega} d\omega' \qquad (15)$$

Based on the catalog of measured SO_2 absorption lines [*Poynter and Pickett*, 1985], the absorption coefficient at a given frequency is calculated with the knowledge of temperature and pressure. With $\sqrt{\epsilon_r'} \approx 1$ as suggested by *Ho et al.* [1966], the imaginary part of the relative permittivity ϵ_r'' is obtained as:

$$\alpha = \frac{2\pi}{\lambda_0}\sqrt{\epsilon_r'}\tan\delta \approx \frac{2\pi}{\lambda_0}\epsilon_r'' \qquad (16)$$

Since ϵ_r'' cannot be known over the whole frequency range, to use this approach, the convergence of $\frac{\epsilon_r''(\omega')}{\omega' - \omega}$ in equation (15) is examined. This convergence can be seen in Figure 1a, showing ϵ_r'' vs. frequency at a temperature of 0°C and pressure of 1 atm, based on the calculation absorption lines up to 7.68 THz. By using the estimated value for $\epsilon_{r\infty} \approx 1.0013$ from *Cuthbertson* [1908] and static value of $\epsilon_r' = 1.0093$ at $T = 10°C$ and $\epsilon_r' = 1.0053$ at $T = 100°C$ in the work of *Gupta* [2001], the calculated dielectric constant in X band is shown in Figure 1b at $T = 0°C$ and pressure of 1 atm. From this, the dielectric constant at 9.6 GHz is estimated to be 1.1423.

[31] Dependence of the dielectric constant of SO_2 on temperature and pressure is required for finding the polarization of the mixture as well. As the polarizability and permanent dipole moment of material are the molecular properties, the following relation between dielectric constant and molecular properties is not expected to change for different frequencies.

$$\frac{(2\epsilon_r' + 1)(\epsilon_r' - 1)}{9\epsilon_r'} = \frac{4\pi N_0 d}{3M}\left(\alpha_T + \frac{\mu^2 g}{3kT}\right) \qquad (17)$$

where N_0 is the Avogadro's number, d is the density in g/m^3, M is the molecular weight in g, k is the Boltzmann constant, α_T is the molecular polarizability, μ is the molecular dipole moment, g is the Kirkwood correlation factor that equals 1 for the gas phase. By knowing the permanent dipole moment $\mu_{SO_2} = 1.63D$ [*Janssen and Poynter*, 1981] (D is the unit 'Debye' for electric dipole moment, $D = 3.33564 \times 10^{-30}$ C · m), the polarizability can be calculated from the above ϵ_r' at $T = 0°C$ and pressure of 1 atm. The dielectric constant and polarization of SO_2 at other temperatures and pressures are consequently known.

Table 3. First Absorption Line and Composition of HCl, SO, and HF[a]

Properties	HCl	SO	HF
First absorption line	625.9 GHz	13.043 GHz (weak)	1232.476 GHz
Maximum concentration	0.5 ppm	0.02 ppm	0.007 ppm

[a]Source: *Poynter and Pickett* [1985].

[32] Dispersion effect of SO_2 can hardly be observed after mixing into the atmosphere model, due to its small volume fraction (maximum 150 ppm). The latest SO_2 mixing ratio profile from the clouds' top down to the surface is given by *Bertaux et al.* [1996] from the Vega mission. The SO_2 distribution in the Venus mesosphere was recently updated by the Venus Express data [*Belyaev et al.*, 2008] with the amount less than 1 ppm. These profiles are still being updated, hence, despite its very small effect, the SO_2 contribution is kept in the overall atmospheric dielectric constant model to allow future updates and applicability to other planetary atmospheres.

2.1.4.3. Gaseous Sulfuric Acid

[33] The X band refractivity of gaseous sulfuric acid (H_2SO_4) has been reported by *Kolodner and Steffes* [1998]. The measurements were carried at frequencies of 8.39 GHz and 8.78 GHz under temperature of 553 Kelvin. The density was known by measuring the volume of vaporized solution into the resonator [*Kolodner and Steffes*, 1998, Table 5]. The averaged density-normalized refractivity was obtained as $(3.086 \pm 0.272) \times 10^{-16}$ [*Kolodner and Steffes*, 1998]. Using equation (17), the polarizability can be calculated for above temperature and density, with $g = 1$ and $\mu_{H_2SO_4} = 2.725$D [*Kuczkowski et al.*, 1981]. Thereby, the polarization of H_2SO_4 at other temperatures and densities can be obtained from the same equation. The effect of mixing gaseous H_2SO_4 into the atmosphere model is found to be quite small with very low dispersion.

2.1.4.4. Carbon Monoxide

[34] According to *Poynter and Pickett* [1985], carbon monoxide (CO) has a weak rotational line at 115.27 GHz. With a low concentration of CO of maximum 36 ppm under the clouds, it can be assumed that in X band, there is no discernable microwave absorption and dispersion due to CO in the Venusian atmosphere. Hence, the effect of CO on ϵ_r'' can be ignored. For its effect on ϵ_r', the static value is used. According to *Bohnet et al.* [2010], the static dielectric constant of CO is 1.000634 at temperature of 298 K and pressure of 1 atm. Carbon monoxide has the molar volume of $v_m = 2.4463 \times 10^4$ cm^3/mol under these conditions, which is used as the characteristic volume for the polarization mixing calculation. Using equation (17) and the CO dipole moment of 0.112 D, its polarizability α_T is calculated from the above permittivity value, and the permittivity at other temperatures and densities is consequently obtained. Shown in the work of *Vandaele et al.* [2008], the mixing ratio of CO increases with altitude and can reach 10^4 ppm at about 125 km. Therefore, though its effect is still small due to the low atmosphere density at this altitude, CO is not a negligible constituent for model completeness.

2.1.4.5. Carbonyl Sulfide

[35] According to *Poynter and Pickett* [1985], Carbonyl Sulfide (OCS or COS) has absorption features covering the microwave spectrum. Its absorption lines start at 12.163 GHz with the repetition period of 12.163 GHz. The line at 12.163 GHz has the line intensity of 4.8933×10^{-7} nm^2 MHz (compare to the weak absorption line of water at 22.235 GHz with intensity of 1.3243×10^{-6} nm^2 MHz). The next absorption line is at 24.326 GHz with intensity of 3.9030×10^{-6} nm^2 MHz. Since the first absorption line is near X band, its effects need to be investigated.

[36] The method to estimate the OCS effect on the dielectric constant is similar as the one applied for SO_2. The Lorentzian function is utilized as the line-shape function and the line width factor of OCS used is 6.4 MHz/torr as determined by *Kolbe et al.* [1977]. With the *Poynter and Pickett* [1985] catalog, the simulation shows a negligible dispersion effect of OCS within X band. With the small fraction of 14 ppm, the variation due to OCS in the overall dielectric constant is in the order of 10^{-5}.

2.1.4.6. Other Trace Gases

[37] The other trace gases given by *de Bergh et al.* [2006] with possible effects on the atmospheric permittivity are HCl, SO and HF. Their first absorption lines and compositions are listed in Table 3. Among them, SO has one weak absorption line near X band. However, due to its trivial amount and based on the previous analysis of OCS, its effect on the dielectric constant is expected to be negligible.

2.1.5. Polarization of the Cloud Layer

[38] So far, only the gaseous components in the Venus atmosphere have been discussed. In the lower part of the atmosphere (~40 km to 58 km [*James et al.*, 1997]), there is a cloud layer containing liquid sulfuric acid droplets with considerable absorption in the microwave region. Its effect on the dielectric constant is discussed here first.

[39] The particle size distribution of Venus' cloud is bimodal in the upper layer, and trimodal or possibly also bimodal in the middle and lower regions [*Knollenberg and Hunten*, 1980; *James et al.*, 1997]. Shown by *Knollenberg and Hunten* [1980] and *James et al.* [1997], the radius of these particles are on the order of micrometers, therefore their X band scattering is negligible. The permittivity of the cloud layer is modeled as distributed liquid sulfuric acid droplets.

[40] In the work of *James et al.* [1997], the mass mixing ratio of both cloud droplets and cloud nuclei are

Table 4. Concentration Versus Density for Sulfuric Acid[a]

Weight Percentage (%)	Density (g/cm^3)
0.5	1.0016
1.0	1.0049
2.0	1.0116
3.0	1.0183
4.0	1.0250
5.0	1.0318
6.0	1.0385
7.0	1.0453
8.0	1.0522
9.0	1.0591
10.0	1.0661
12.0	1.0802
14.0	1.0947
16.0	1.1094
18.0	1.1245
20.0	1.1398
22.0	1.1554
24.0	1.1714
26.0	1.1872
28.0	1.2031
30.0	1.2191
32.0	1.2353
34.0	1.2518
36.0	1.2685
38.0	1.2855
40.0	1.3028
42.0	1.3205
44.0	1.3386
46.0	1.3570
48.0	1.3759
50.0	1.3952
52.0	1.4149
54.0	1.4351
56.0	1.4558
58.0	1.4770
60.0	1.4987
70.0	1.6105
80.0	1.7272
90.0	1.8144
92.0	1.8240
94.0	1.8312
96.0	1.8355
98.0	1.8361
100.0	1.8305

[a]Temperature is 20°C. Source: *Lide* [2000].

provided, noted here as $M_{droplet}$ and M_{nuclei} in ppm or mg/kg. By subtracting the mass mixing ratio of the cloud nuclei from that of cloud droplets, the mass mixing ratio of the distributed H_2SO_4-H_2O solution in the Venus cloud, $M^{distr}_{H_2SO_4-H_2O}$, is obtained. This mass mixing ratio together with the Venusian atmosphere density gives the density of the distributed H_2SO_4-H_2O solution in the Venus cloud layer as shown in equation (18).

$$\rho^{distr}_{H_2SO_4} = M^{distr}_{H_2SO_4-H_2O} \cdot \rho_{atm} = \left(M_{droplet} - M_{nuclei}\right) \cdot \rho_{atm} \tag{18}$$

where ρ_{atm} is the atmosphere density in kg/m^3 and $\rho^{distr}_{H_2SO_4}$ is the distributed H_2SO_4-H_2O solution density in mg/m^3 in the Venus cloud.

[41] Furthermore, the relation between the H_2SO_4-H_2O solution density and its concentration, or H_2SO_4 weight percentage, has been measured at 20°C and provided by *Lide* [2000] as shown in Table 4. This relation is adapted to the temperature range at the cloud layer (~250 K to 400 K), since according to the H_2SO_4-H_2O solution permittivity measurement as a function of concentration in the work of *Cimino* [1982], its real part, or volumetric polarization, has little dependence on temperature for higher concentrations (>80%), which includes the concentration range of the H_2SO_4-H_2O solution in the Venus cloud (~80% to 99%) [*James et al.*, 1997]. Using this density-concentration relation, the concentrated H_2SO_4-H_2O solution density $\rho^{concentr}_{H_2SO_4}$ (in g/cm^3) corresponding to the concentration profile in the Venus cloud [*James et al.*, 1997] can be found. The ratio between $\rho^{concentr}_{H_2SO_4}$ and $\rho^{distr}_{H_2SO_4}$ in the cloud layer is defined as a spreading factor η_s,

$$\eta_s = \frac{\rho^{concentr}_{H_2SO_4}}{\rho^{distr}_{H_2SO_4}} \cdot 10^{-9} \tag{19}$$

Therefore, the polarization of the distributed H_2SO_4-H_2O solution in the cloud layer can be calculated by dividing the polarization of the concentrated H_2SO_4-H_2O solution, which is obtained from its measured dielectric constant at X band [*Cimino*, 1982], by the spreading factor:

$$P^{distr}_{H_2SO_4-H_2O} = \frac{P^{concentr}_{H_2SO_4-H_2O}}{\eta_s} \tag{20}$$

where $P^{distr}_{H_2SO_4-H_2O}$ and $P^{concentr}_{H_2SO_4-H_2O}$ are the volumetric polarization of the distributed H_2SO_4-H_2O solution in the cloud layer and the concentrated H_2SO_4-H_2O solution, respectively. As the mass mixing ratio of the cloud nuclei is much smaller than the H_2SO_4-H_2O solution, its polarization is neglected. The polarization of the distributed H_2SO_4-H_2O solution is taken as the polarization of the cloud layer P_{cloud}.

[42] Considering the cloud droplets as a part of the atmospheric fluid, their polarization was added into the total polarization of the atmosphere mixture in a similar way as for the gaseous components. The density of droplets is assumed not to change before and after being incorporated into the mixture of gaseous components and droplets. The volume fraction of droplets Φ_{cloud} is the

inverse of the spreading factor. Thereby, polarization of the cloud layer can be directly included into total polarization as:

$$P_{mix} = \sum_{gaseous} \Phi_i^* P_i\left(T,\ \frac{\rho_{i,mix}}{v_i^*}\right) + \Phi_{cloud} P_{cloud}(\rho) \quad (21)$$

The first term above is the same as the one discussed previously in the mixing approach based on the constant temperature and reduced density; the second term is the polarization from clouds. The overall dielectric constant of Venus' atmosphere is obtained from the total polarization by equation (3).

2.1.6. Polarization of the Ionosphere

[43] An ionosphere exists in Venus' atmosphere above 100 km, where the density of gases becomes very small. The ionosphere is a plasma medium. Assuming only interaction between free electrons and electromagnetic waves, the expression for the dielectric constant of plasma can be written as [*Kong*, 1990]:

$$\epsilon(\omega) = \epsilon_0\left(1 - \frac{\omega_p^2}{\omega^2}\right) \quad (22)$$

where the plasma frequency ω_p is

$$\omega_p = \sqrt{\frac{Nq^2}{\epsilon_0 m}} \approx 56.4\sqrt{N} \quad (23)$$

N is the electron density in m^{-3}, $q = -1.6 \times 10^{-19}$ C; electron mass $m = 9.1 \times 10^{-28}$ g; $\epsilon_0 = 8.854 \times 10^{-12}$ F/m. Based on the electron density information provided by *Pätzold et al.* [2007], the dielectric constant profile of the ionosphere is modeled. As the dielectric constant due to the atmospheric gases can be approximated as 1 above 100 km, the overall dielectric constant profile can be constructed by superposition of the profiles modeled from the ionosphere above 100 km and from atmospheric gases and clouds below 100 km. Small amounts of dispersion due to the ionosphere can be seen in Figure 2, showing the differences between the dielectric constant profiles at 5 frequencies and the values at 9.6 GHz. The ionosphere electron density distribution along altitudes varies with time and location and the profile used in this estimation is according to the typical Venus ionospheric electron density height profile derived from the VeRa occultation data [*Pätzold et al.*, 2007].

2.2. Imaginary Part of Permittivity

[44] The imaginary part of the relative permittivity, ϵ_r'', can be extracted from the total absorption of the Venusian atmosphere at X band. With the assumption that $\epsilon_r'' \ll \epsilon_r'$ and the relative permeability $\mu_r \approx 1$, the field absorption coefficient is [*Ulaby et al.*, 1981]

$$\alpha_f = \frac{2\pi}{\lambda_0}\left\{\frac{\mu_r\epsilon_r'}{2}\left[\sqrt{1 + \left(\frac{\epsilon_r''}{\epsilon_r'}\right)^2} - 1\right]\right\}^{1/2} \approx \frac{2\pi}{\lambda_0}\left\{\frac{\mu_r\epsilon_r'}{2}\left[\frac{1}{2}\left(\frac{\epsilon_r''}{\epsilon_r'}\right)^2\right]\right\}^{1/2} \approx \frac{\pi}{\lambda_0}\sqrt{\epsilon_r'}\tan\delta \quad (24)$$

where $\tan\delta = \epsilon_r''/\epsilon_r'$ is the loss tangent. This coefficient has the unit of one over the unit of length. The power absorption coefficient, or absorptivity, which is twice the above absorption coefficient, is noted as α,

$$\alpha = \frac{2\pi}{\lambda_0}\sqrt{\epsilon_r'}\tan\delta = \frac{2\pi}{\lambda_0}\frac{\epsilon_r''}{\sqrt{\epsilon_r'}} \quad (25)$$

By knowing the total microwave absorption and modeling the dielectric constant of Venus' atmosphere as described previously, the imaginary part of the permittivity is obtained. The total absorption of the atmosphere can be found to good approximation by summing up absorptions of each component in the mixture. Note that the unit of above absorption coefficient is cm^{-1}, which is often used in physics and astronomy. It has the relation of 1 cm^{-1} = 0.5 Np/cm = 0.5×10^3 Np/km = 4.343×10^3 dB/km [*Steffes and Eshleman*, 1981a], the latter unit is commonly used in the papers being referenced below.

2.2.1. Absorption of CO_2, N_2, Ar, and H_2O

[45] In the work of *Ho et al.* [1966], total absorption of CO_2, N_2, Ar and H_2O mixture has been modeled based on laboratory measurement results. It is expressed as:

$$\alpha = P^2\overline{\nu}^2\left(\frac{273.15}{T}\right)^5\left(15.7f_{CO_2}^2 + 3.90f_{CO_2}f_{N_2} + 2.64f_{CO_2}f_{Ar} + 0.085f_{N_2}^2 + 1330f_{H_2O}\right)\times 10^{-8}\ \mathrm{cm}^{-1} \quad (26)$$

with $\rho = P\frac{273.15}{T}$, wave number $\overline{\nu} = \frac{1}{\lambda_0}$ and P is pressure in atm. The quantities f_{CO_2}, f_{N_2}, f_{Ar} and f_{H_2O} are the molar fractions of CO_2, N_2, Ar and H_2O, respectively.

2.2.2. Absorption of SO_2

[46] The SO_2 molecule is an asymmetric rotor with a rich rotational spectrum extending throughout the microwave region; therefore, the microwave absorption of SO_2 is significant. *Janssen and Poynter* [1981] provide a theoretical model describing this absorption, and *Steffes and Eshleman* [1981b] give a model based on the laboratory measurements simulating the temperature and pressure

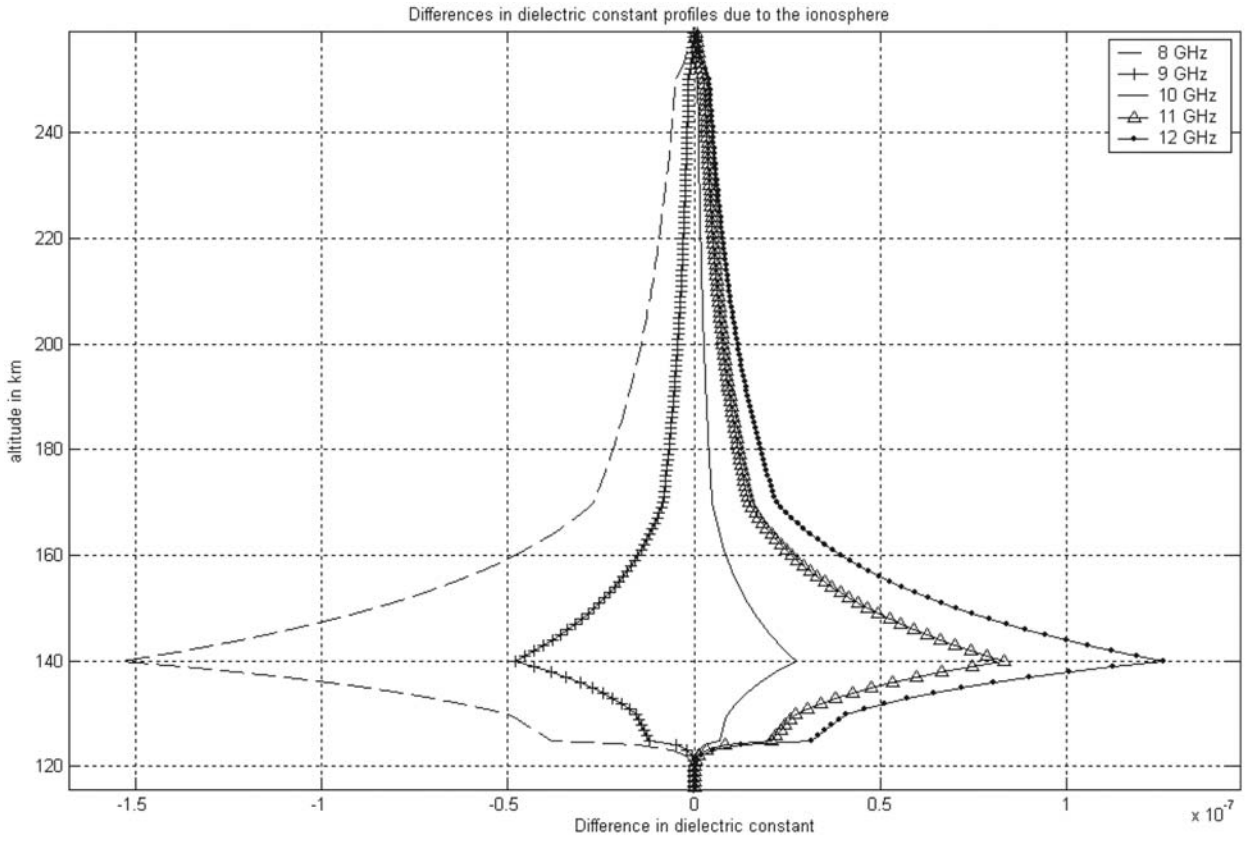

Figure 2. Dispersion due to the ionosphere. Differences are taken by subtracting values at five frequencies from value at 9.6 GHz. The electron density profile uses VeRa occultation observation [*Pätzold et al.*, 2007].

at the layer containing SO_2 in the Venus atmosphere. However, in the recent literature, *Suleiman et al.* [1996] mention that the *Steffes and Eshleman* [1981b] model is not an optimal fit to the measured results at all frequencies and that the frequency dependence is not uniformly valid due to measurement errors. In the same paper, *Suleiman et al.* [1996] present detailed laboratory measurements of gaseous SO_2 in CO_2 under pressure of 1 to 4 atm and temperature from 290 to 505 K at frequencies of 2.25 GHz, 8.5 GHz, and 21.7 GHz. The Ben-Reuven line shape expression was used in their modeling. The *Suleiman et al.* [1996] model is used in the atmosphere model developed here.

[47] The absorption at frequency ν due to a single rotational resonant line at frequency ν_0 is,

$$\alpha = \alpha_{\max}\pi\gamma F_{shape}(\nu, \nu_0, \cdots) \text{ cm}^{-1} \tag{27}$$

where ν and ν_0 are in MHz, γ is the linewidth in MHz, and F_{shape} is the spectral line shape function in MHz^{-1}. The quantity $\alpha_{\max}$ is the absorption at the line center,

$$\alpha_{\max} = 102.46\frac{P_{SO_2}}{\gamma}I(T_0)\left(\frac{T_0}{T}\right)^{7/2} e^{-\left(\frac{hc}{k}\right)E_l\left(\frac{1}{T}-\frac{1}{T_0}\right)} \text{ cm}^{-1} \tag{28}$$

where P_{SO_2} is the partial pressure of SO_2 in torr (1 torr = 1/760 atm), $I(T_0)$ is line center intensity in nm^2 MHz at T_0 = 300 K, E_l is the lower state energy in cm^{-1}, k is the Boltzmann's constant 1.38×10^{-23} J/K, h is the Planck's constant 6.63×10^{-34} J · s, and c is the speed of light 3×10^{10} cm/s in free space. The total absorption coefficient at a given frequency can be obtained by summing up all the line contributions to this frequency. The absorption spectrum up to 750 GHz has been covered in this calculation, which is obtained from *Poynter and Pickett*

Table 5. Parameters for Ben-Reuven Line Shape Function[a]

γ_{SO_2/CO_2}	γ_{SO_2/SO_2}	ζ_{SO_2/CO_2}	ζ_{SO_2/SO_2}	δ_{SO_2}	$m = n$
7.2 MHz/torr	16 MHz/torr	1.3 MHz/torr	1.6 MHz/torr	2.9 MHz/torr	0.85

[a]Source: *Suleiman et al.* [1996].

[1985]. The line shape function F_{shape} in equation (27) is substituted by the Ben-Reuven expression,

$$F_{shape} = F_{BR}(\nu, \nu_0, \gamma, \zeta, \delta) = \frac{2}{\pi}\left(\frac{\nu}{\nu_0}\right)^2 \cdot \frac{(\gamma-\zeta)\nu^2 + (\gamma+\zeta)\left[(\nu_0+\delta)^2+\gamma^2-\zeta^2\right]}{\left[\nu^2-(\nu_0+\delta)^2-\gamma^2+\zeta^2\right]^2+4\nu^2\gamma^2} \text{ MHz}^{-1} \quad (29)$$

where the linewidth γ is

$$\gamma = \left(\gamma_{SO_2/CO_2}\right)P_{CO_2}\left(\frac{T_0}{T}\right)^n + \left(\gamma_{SO_2/SO_2}\right)P_{SO_2}\left(\frac{T_0}{T}\right)^n \text{ MHz} \quad (30)$$

and the coupling element ζ is

$$\zeta = \left(\zeta_{SO_2/CO_2}\right)P_{CO_2}\left(\frac{T_0}{T}\right)^m + \left(\zeta_{SO_2/SO_2}\right)P_{SO_2}\left(\frac{T_0}{T}\right)^m \text{ MHz} \quad (31)$$

The frequency shift δ is given by

$$\delta = \delta_{SO_2}P_{SO_2} \text{ MHz} \quad (32)$$

The foreign gas broadened linewidth parameter γ_{SO_2/CO_2}, the self-broadened linewidth parameter γ_{SO_2/SO_2}, the foreign gas coupling parameter ζ_{SO_2/CO_2}, the self-coupling parameter ζ_{SO_2/SO_2}, the frequency shift parameter δ_{SO_2}, temperature dependence of linewidth n, and the temperature dependence of coupling element m are given in Table 5.

2.2.3. Absorption of H_2SO_4

[48] Early laboratory measurements by *Steffes* [1985] indicate that the dominant microwave absorber at S band and X band in the 10 km region below the Venus cloud layer (approximately 38 to 48 km) is H_2SO_4. The model provided in that paper was later updated by *Kolodner and Steffes* [1998] with improved measurements that provide a better fit model. The absorptivity α is normalized to the number mixing ratio q, which is the ratio of the number of H_2SO_4 molecules in the H_2SO_4/CO_2 mixture, to give an expression over all pressures and frequencies:

$$\frac{\alpha}{q} = 53.601p^{1.11}f^{1.15}\left(\frac{553}{T}\right)^{3.0\pm0.2} \text{ dB km}^{-1} \quad (33)$$

where f is frequency in GHz, p is pressure in atm and T is temperature in Kelvin.

[49] Gaseous H_2SO_4 thermally dissociates into SO_3 and H_2O at altitudes between 35 and 40 km. The microwave absorption of dissociates (H_2O and SO_3) is negligible in these small amounts when compared to the microwave absorption of the H_2SO_4 vapor. As shown by the simulation results in Figure 3, both SO_2 and H_2SO_4 have noticeable effects on the microwave absorption. At 35 km to 50 km where H_2SO_4 exists, the curve shows a large effect due to H_2SO_4, though its mixing ratio is less than 5 ppm.

2.2.4. Absorption of Other Trace Gases

[50] Among the other trace gases, only OCS is considered in the absorption model here, for it has periodically repeated absorption lines near X band. As mentioned previously in the dielectric constant modeling, the Lorentzian function is utilized as the line-shape function and the line width factor of OCS is using 6.4 MHz/torr as determined by *Kolbe et al.* [1977]. With the absorption line data provided by *Poynter and Pickett* [1985], absorption of OCS in X band can be calculated by adding up the absorption contributions from every line by equations (27) and (28). As discussed previously, the other minor gaseous constituents, e.g., CO, HCl, SO, HF, etc., have negligible absorption in X band.

2.2.5. Absorption of Cloud Layer

[51] The absorption of the cloud droplets is investigated using the measured imaginary permittivity of the H_2SO_4-H_2O solution in the work of *Cimino* [1982], as well as the spreading factor defined in the previous cloud layer polarization modeling section.

[52] Shown in the results measured at temperature between about 295 K and 376 K [*Cimino*, 1982], which covers the temperature range in the Venus cloud layer, the value of the imaginary part of the relative permittivity ϵ_r'' varies little as a function of concentration in the 80% to 95% range and can be assumed to be concentration-independent when the H_2SO_4 weight percentage is in that range; it decreases as the concentration increases from 95% to ~99%. The dependence on temperature of ϵ_r'' is

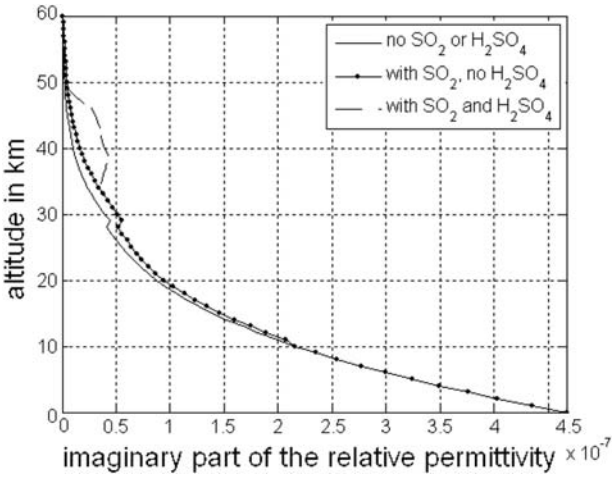

Figure 3. Comparison of effects of including SO_2 and H_2SO_4 on the imaginary part of the relative permittivity at 9.6 GHz. The mixing ratio of SO_2 is up to 130 ppm, while the mixing ratio of H_2SO_4 is only up to 5 ppm.

modeled by fitting the X band ϵ_r'' measurement data for H_2SO_4-H_2O solution with different concentration provided by *Cimino* [1982]. The resulting expression shows linear dependence on temperature as,

$$\epsilon_T'' = \kappa(T - 295) + \epsilon_{295K}'' \tag{34}$$

where κ is about 1.17 for H_2SO_4-H_2O solution with concentration between 80% and 95% and is assumed to be linearly decreasing from 1.17 to 0.85, which gives a good fit for concentration of ~99%.

[53] Using the ϵ_r'' value obtained above together with the ϵ_r' value of the concentrated H_2SO_4-H_2O solution, which has been discussed in the cloud layer polarization modeling section, the absorption coefficient corresponding to the temperature and concentration profile in the cloud layer can be calculated using equation (24) for the concentrated H_2SO_4-H_2O solution. By dividing this absorption by the spreading factor, the absorption coefficient of the cloud layer is obtained and added into the total absorption of the Venusian atmosphere.

3. Model Verification

3.1. Standard Atmospheric Profiles and Results

[54] To verify the Venus atmospheric permittivity model, profiles of temperature, pressure (or density), electron density of the ionosphere, composition of atmospheric gases, mass content and concentration of the cloud droplets in Venus' atmosphere are required. These profiles vary at different locations, in particular, at different latitudes [*Cimino*, 1982; *Seiff et al.*, 1985; *Marcq et al.*, 2008; *Zasova et al.*, 2006], thus a comprehensive parametric model is generated here that could be used for simulations

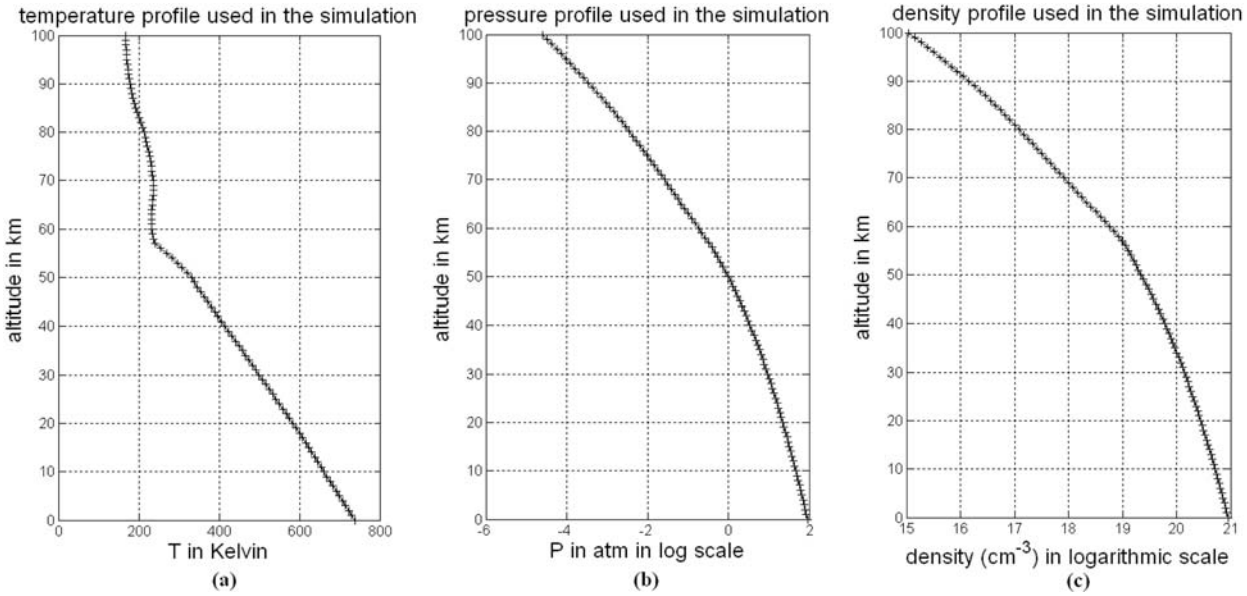

Figure 4. Profiles used in the simulation: (a) temperature profile using the measurement data at latitude of 75° in the work of *Seiff et al.* [1985] after its being increased by 3 K [*Zasova et al.*, 2006; *James et al.*, 1997], (b) pressure profile [*Seiff et al.*, 1985], and (c) density profile [*Seiff et al.*, 1985].

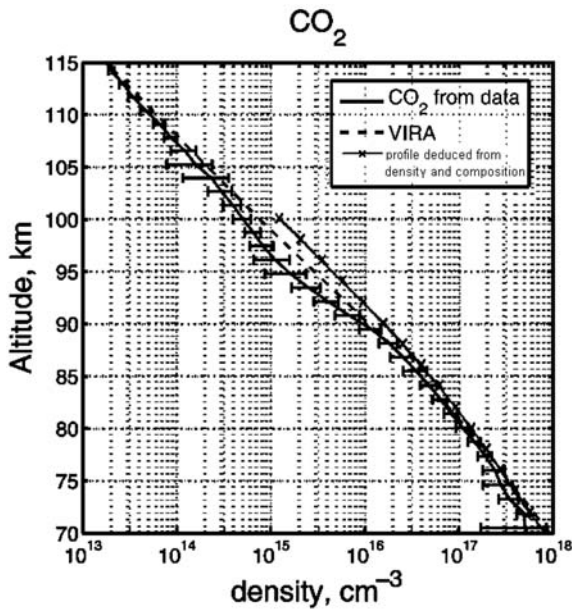

Figure 5. Comparison between CO_2 density profile constructed assuming constant composition of 96.5% (solid line with crosses), VIRA model [*Keating et al.*, 1985] (dashed line), and the measured CO_2 density profile from Venus Express [*Fedorova et al.*, 2008] (solid line) in the Venus mesosphere.

based on information provided in the literature, or as new atmospheric information becomes available.

[55] The temperature profiles at different latitudes [*Seiff et al.*, 1985] show steady values under the clouds but vary above 40 km and these profiles have been further updated by the proceeding Venusian missions [*Moroz and Zasova*, 1997]. For the lower atmosphere (62 km down to the surface), the temperature and pressure profiles were measured with higher accuracy by VEGA spacecraft [*Zasova et al.*, 2006]. Particularly, the vertical profiles below 12 km were obtained with sufficient accuracy for the first time [*Zasova et al.*, 2006]. The temperature measured by VEGA-2 at the same pressure is approximately 3 to 4 K warmer than the profile of *Seiff et al.* [1985]. Recently, the temperature profile is further measured by the Venus Express mission [*Pätzold et al.*, 2007; *Tellmann et al.*, 2009]. However, since the latest measurement data set was not available to us, the profiles before Venus Express are taken as the standard temperature profile input for the model simulation. First, for the lower atmosphere, since most atmospheric profiles are available at higher latitudes, the temperature curve at latitude of 75° in the work of *Seiff et al.* [1985] is used after being increased by 3 K [*James et al.*, 1997] as the 'standard' temperature profile. The pressure and density profiles of *Seiff et al.* [1985] are included in the 'standard' lower atmosphere model. For the middle atmosphere, the profiles have been updated by the Magellan radio eclipse

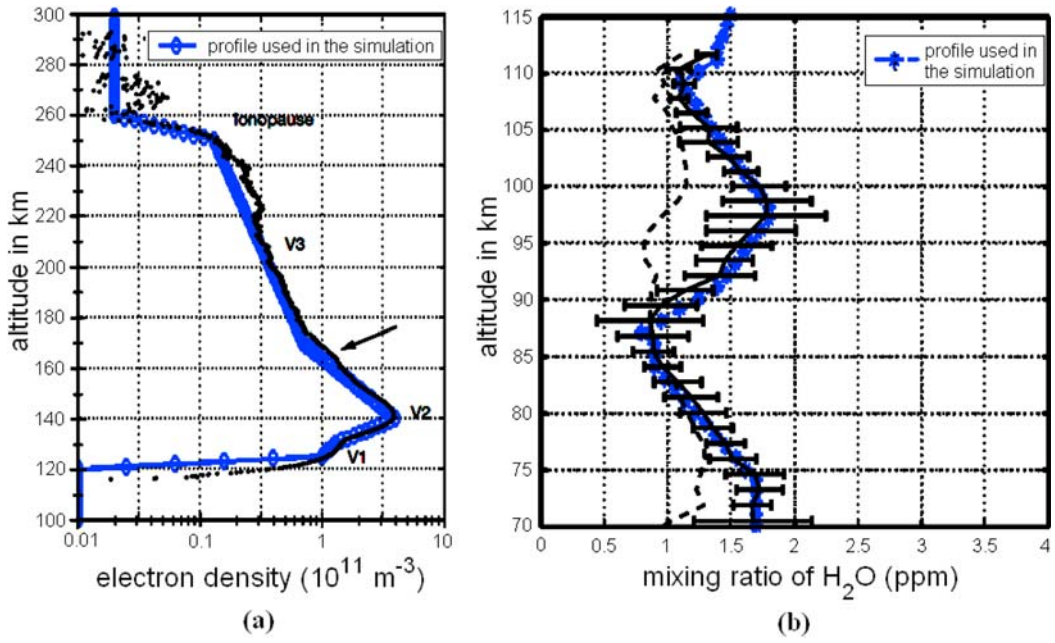

Figure 6. Standard profiles of (a) electron density (compared with the Venus Express observation [*Pätzold et al.*, 2007]) and (b) water vapor (compared with the Venus Express observation [*Vandaele et al.*, 2008]).

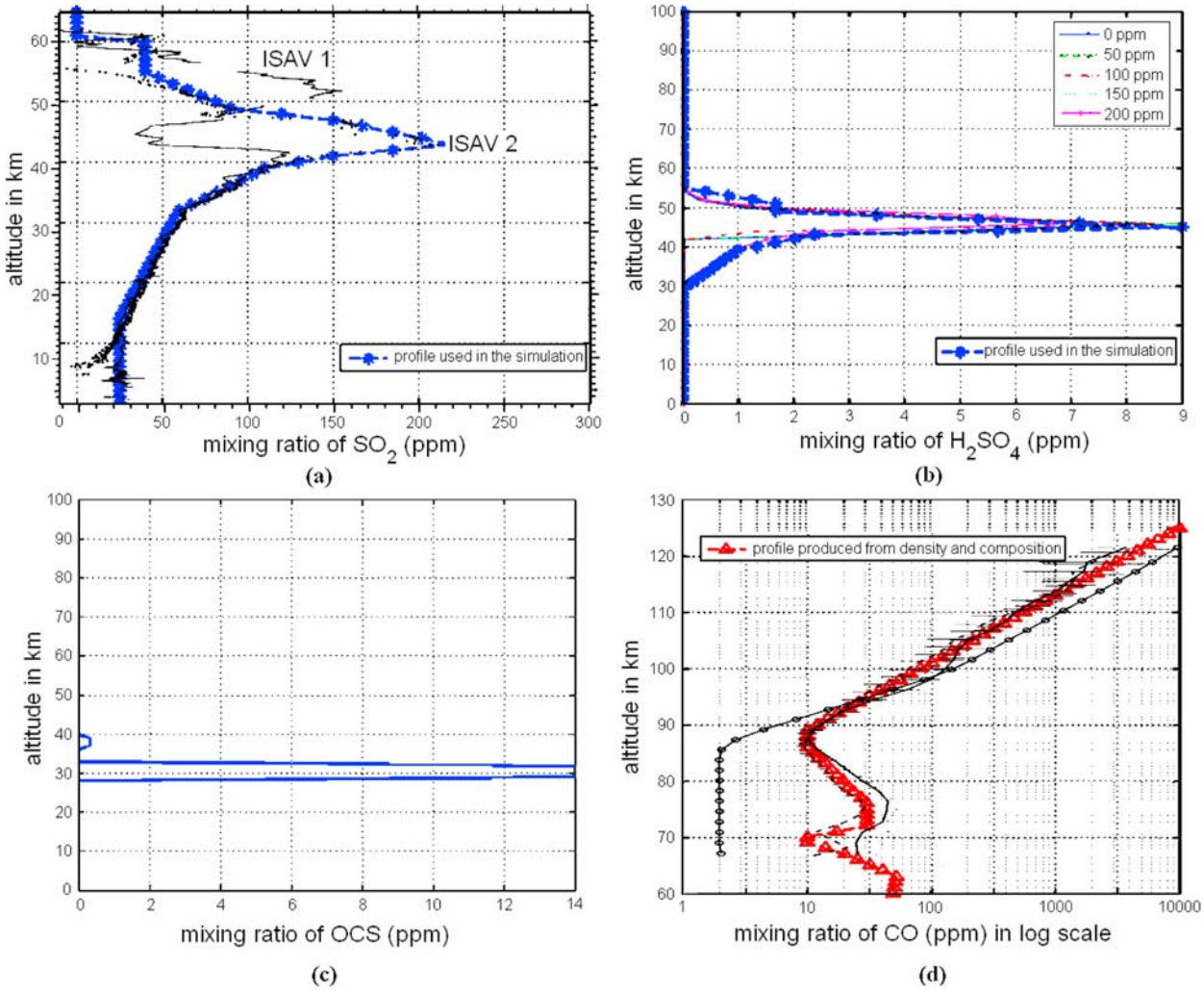

Figure 7. Standard profiles for (a) SO_2 (together with profiles measured by ISAV 1 and ISAV 2 in the VEGA mission [*Bertaux et al.*, 1996]), (b) H_2SO_4 (together with the retrieved profiles from the VLA observation; they are obtained assuming different SO_2 abundance [*Jenkins et al.*, 2002]), (c) OCS (from the ground observation [*Svedhem et al.*, 2007]), and (d) CO (together with the profiles measured at different locations by Venus Express mission [*Vandaele et al.*, 2008]).

experiments and Venera 15, 16 observations [*Zasova*, 1995; *Zasova et al.*, 2006]. In the simulation, the middle atmosphere temperature and pressure profiles are using the column of L_s = 200°–270° in Table 5 of *Zasova et al.* [2006] to have the closer conditions as Magellan occultation data used in the model verification. The density profile in the middle atmosphere can be obtained by the equation of state of ideal gas. These 'standard' atmosphere profiles are shown in Figure 4. The main constituents in Venus' atmosphere are generally accepted as 96.5% CO_2 and 3.5% N_2 in volume fractions. The validity of the assumption of a constant mixing ratio of these major gases is shown in Figure 5, where the density profile of CO_2 obtained under this assumption is compared with the density of CO_2 in the Venus mesosphere from VIRA and measured by Venus Express [*Fedorova et al.*, 2008]. It shows a larger discrepancy above 80 km. Hence, in the simulation, this assumption is only applied at altitudes up to 80 km. For higher altitudes, the VIRA profile for CO_2 density is used since the Venus Express data set is not currently available to us.

[56] The electron density profile of the ionosphere is built according to *Pätzold et al.* [2007] as shown in Figure 6a. The ionosphere structure on Venus varies with latitudes,

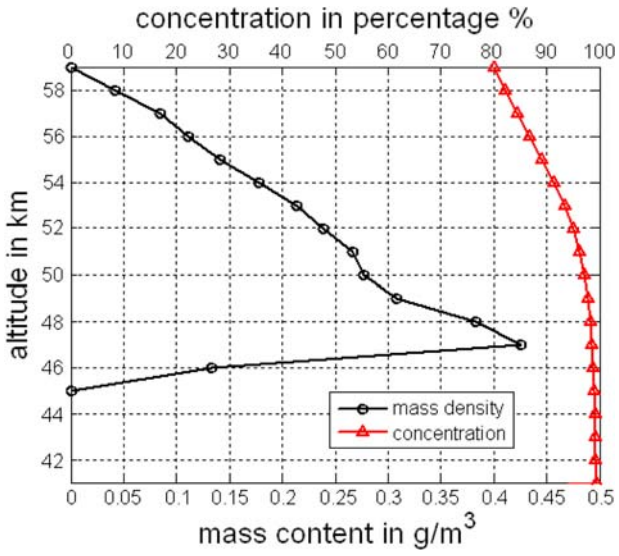

Figure 8. Standard profiles for the mass content and concentration of cloud (according to the Pioneer Venus observation [*Knollenberg and Hunten*, 1980; *James et al.*, 1997]).

local time, solar activity, etc. [*Pätzold et al.*, 2007]. Therefore, local profiles of electron density should be used in the applications requiring higher accuracy. Composition of the trace gases under the clouds is based on the mixing ratios listed by *de Bergh et al.* [2006] and illustrated by *Svedhem et al.* [2007]. The latest detailed profile of SO_2 is provided from the VEGA mission [*Bertaux et al.*, 1996], and the one of H_2SO_4 is provided from observation by the Very Large Array (VLA) of the National Radio Astronomy Observatory [*Jenkins et al.*, 2002]. In the work of *Bertaux et al.* [1996], the SO_2 profiles are measured by ISAV, a spectrometer designed to measure the local atmospheric absorption and its detailed spectrum in the ultraviolet range. The ISAV 1 and ISAV 2 instruments are carried on VEGA 1 and VEGA 2, respectively. The SO_2 profile for the model simulation is constructed similar to the measured profile by ISAV 2 as plotted in Figure 7a, since its larger mixing ratio is preferred to estimate the largest possible distortion and absorption on the signal propagation when applying this model in the radar design.

[57] In Figure 7b, the H_2SO_4 profile used in the simulation is shown together with the retrieved abundance profiles given by *Jenkins et al.* [2002]. They were obtained by assuming different SO_2 abundances. Similarly, the largest abundance of H_2SO_4 is selected for the model simulation. The distributions of water vapor, SO_2, and CO in the mesosphere are recently updated by Venus Express data, they are included in the simulation except for SO_2 above the clouds, which is negligible (<1 ppm). Profiles used for H_2O and CO are shown in Figures 6b and 7d, together with the measured values at different locations [*Vandaele et al.*, 2008]. Distribution of OCS is shown in Figure 7c. From recent Venus Express data, *Marcq et al.* [2008] discussed the distribution dispersion of these minor gases with respect to latitude. The data showed a noticeable variation of CO mixing ratio from 24 ppm to 31 ppm at 36 km and small variation (<4 ppm at 33 km) of OCS as well. Given these dispersions with respect to

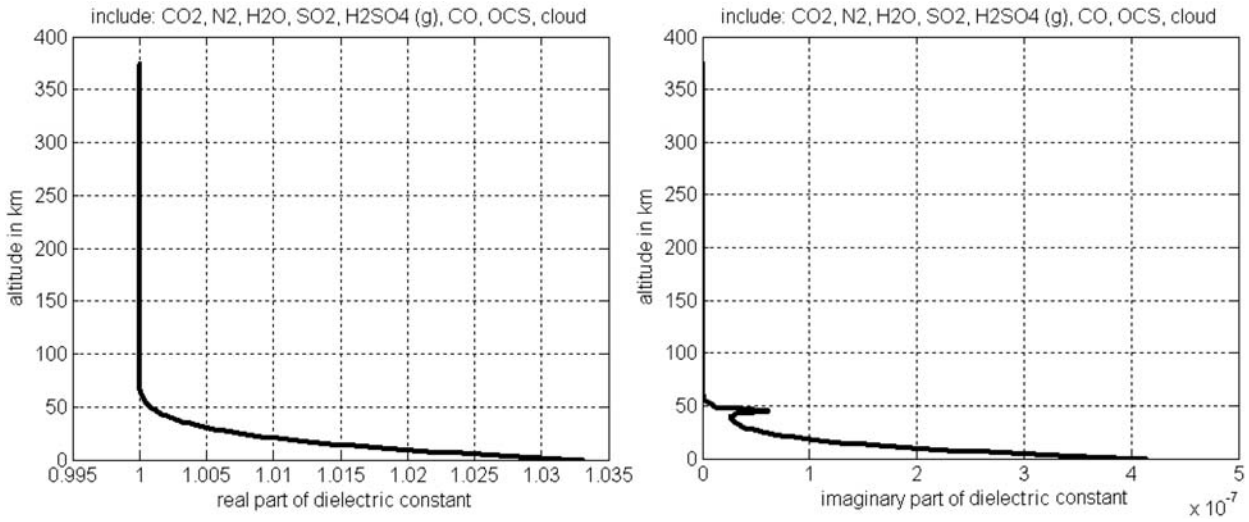

Figure 9. Relative permittivity profiles resulting from the standard atmospheric profiles.

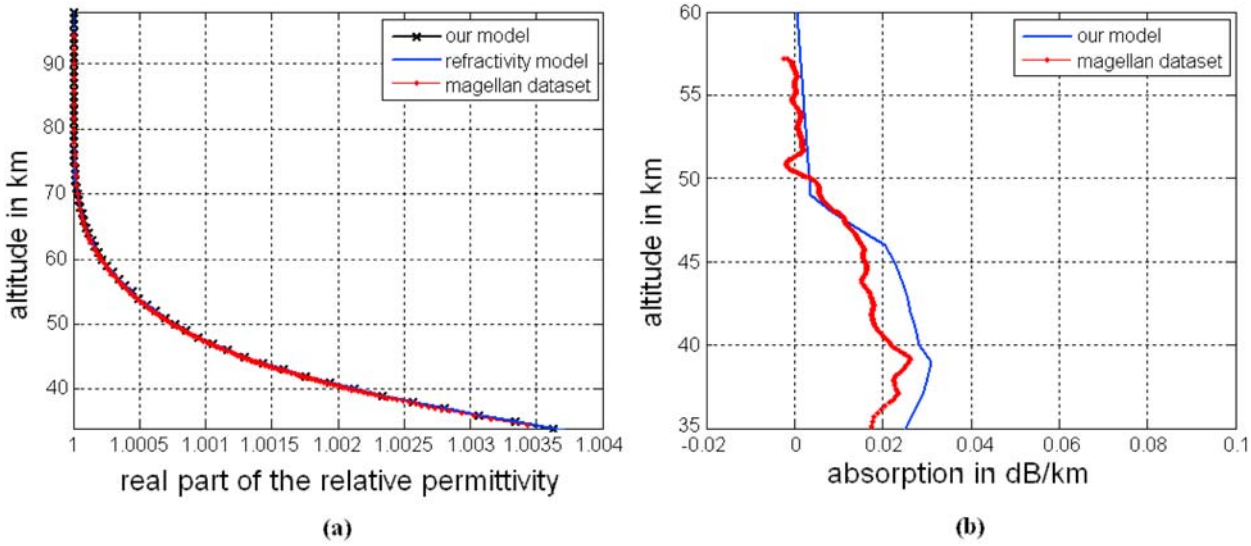

Figure 10. Verification of the relative permittivity: (a) comparison of the dielectric constant result from our model simulation, the result from the radio refractivity model, and the measured data from Magellan; (b) comparison of absorption between model simulation results and the measurement from Magellan (orbit 3212 data set).

location, the dispersion of the atmospheric permittivity can also be estimated using this model. For the cloud layer, the mass mixing ratio of H_2SO_4-H_2O droplets is constructed according to *Knollenberg and Hunten* [1980] and *James et al.* [1997]. With the atmosphere density profile constructed above, the cloud mass density distribution along altitudes is obtained from the cloud mass mixing ratio as shown in Figure 8. Figure 8 also presents the concentration profile of cloud layer used in the model simulation, which is given by *James et al.* [1997].

[58] Above profiles are used as the 'standard' atmospheric profiles for the model simulation in this paper. Resulting relative permittivity profiles are shown in Figure 9.

3.2. Verification of the Model: Real Part of Permittivity

[59] In the work of *Stratton* [1968], radio refractivity of a mixture consisting of CO_2, N_2 and H_2O in the Venusian atmosphere has been described by,

$$N = 134.9\frac{P_{CO_2}}{T} + 80.29\frac{P_{N_2}}{T} + 16.57\left(1 + \frac{5748}{T}\right)\frac{P_{H_2O}}{T} \tag{35}$$

where P_{CO_2}, P_{N_2} and P_{H_2O} are partial pressures of CO_2, N_2 and H_2O in mbar; T is temperature in Kelvin. With the relationship between radio refractivity and refractive index given by $N = 10^6(n - 1)$, and that $\epsilon_r' = n^2$, the dielectric constant is estimated and compared with the model simulation results. The comparison is shown in Figure 10a, in which the result from Magellan orbit 3212 data set is plotted as well. Difference between the simulation result and the one from the radio refractivity model is in the order of 10^{-3}, likely due to errors in assumed temperature and pressure profiles.

[60] In the work of *Jenkins et al.* [1994], absorption profiles of three orbits at frequencies of S band and X band are analyzed in the region of gaseous H_2SO_4. The X band profiles can be used to verify our atmospheric permittivity model in this region. The distribution profiles of H_2SO_4 obtained from the same Magellan orbits [*Kolodner and Steffes*, 1998] are used for model verification here. The results of our model for absorption due to CO_2, SO_2 and H_2SO_4 in this region are compared to the measured results from Magellan orbit 3212 data set as shown in Figure 10b. The calculated absorption is generally consistent with the measured curve. Since the value is affected by the temperature and pressure profiles, as well as the difference between the exact H_2SO_4 profile and values used as the simulation entries, error exists between the simulated results and the measured data. Our simulation slightly overestimates the absorption rates below 45 km.

[61] Since the Magellan data set is the only measured absorption data found, which is from altitude of 35 km to 57 km, absorption profiles in other regions have not been compared. The overall absorption profile gives a one-

way absorption of about 5.62 dB, assuming a nadir look direction from altitude of 200 km. There is no significant contribution to the absorption from SO_2 and CO_2, therefore it is difficult to compare the results due to these two components alone with the existing data.

4. Conclusion and Improvement

[62] In this work, a permittivity model for the Venus atmosphere up to 300 km has been constructed. Using previous Venus observations and data analyses, the model has been simulated and verified. It is shown that the model results are in good agreement with those from available measurements. This model will provide a necessary tool for the analysis of X band electromagnetic wave propagation in the Venus atmosphere, which is critical information needed for the proper design of future orbiting radar systems.

[63] Potential minor improvements to the model presented here could be obtained as follows:

[64] 1. This work uses the equation of state for ideal gas. Instead, the van der Waals equation, which may be more accurate, can be applied.

[65] 2. For several of the atmospheric constituents such as H_2SO_4-H_2O, instead of fitting curves to the available measurements to get the profiles, look-up tables may be more true to the original data and can be utilized if accurate data are available in the whole region of interest.

[66] 3. Accuracy of this atmosphere model can be always improved by new or more reliable measurements from the Venus atmospheric conditions and composition.

[67] A strength of this model is that it accounts for all of the known atmospheric components of Venus, even for the trace gases. The formulation is kept general and flexible, such that the model can be easily updated for pressure, temperature, and composition profiles as these parameters are updated in the future. The model can be applied to any location of interest on Venus as long as the composition and temperature/pressure profiles are given. Furthermore, the model can be easily modified to apply to other planetary bodies.

[68] **Acknowledgments.** This work was performed at the University of Michigan and at the Jet Propulsion Laboratory through support from JPL-DRDF Innovative Spontaneous Concepts program. Additionally, the authors would like to sincerely thank the three anonymous reviewers for their detailed and thorough comments and corrections, which have led to greatly improving the quality of the paper and the model herein.

References

Belyaev, D., O. Korablev, A. Fedorova, J.-L. Bertaux, A.-C. Vandaele, F. Montmessin, A. Mahieux, V. Wilquet, and R. Drummond (2008), First observations of SO_2 above Venus' clouds by means of Solar Occultation in the Infrared, *J. Geophys. Res.*, *113*, E00B25, doi:10.1029/2008JE003143.

Bertaux, J.-L., T. Widemann, A. Hauchecorne, V. I. Moroz, and A. P. Ekonomov (1996), VEGA 1 and VEGA 2 entry probes: An investigation of local UV absorption (220–400 nm) in the atmosphere of Venus (SO_2, aerosols, cloud structure), *J. Geophys. Res.*, *101*(E5), 12,709–12,745.

Birnbaum, G. (1952), The dielectric constant of water vapor in the microwave region, *J. Appl. Phys.*, *23*(2), 220–223.

Boettcher, C. J. F. (1973), *Theory of Electric Polarization*, vol. 1, *Dielectrics in Static Fields*, Elsevier, New York.

Boettcher, C. J. F. (1978), *Theory of Electric Polarization*, vol. 2, *Dielectrics in Time-Dependent Fields*, Elsevier, New York.

Bohnet, M., et al. (2010), *Ullmann's Encyclopedia of Industrial Chemistry*, 7th ed., Wiley-VCH, Weinheim, Germany. (Available at http://mrw.interscience.wiley.com/emrw/9783527306732/home/)

Cimino, J. (1982), The composition and vertical structure of the lower cloud deck on Venus, *Icarus*, *51*, 334–357.

Cuthbertson, C. (1908), On the refractive indices of gaseous nitric oxide, sulphur dioxide, and sulphur trioxide, *R. Soc. Proc.*, *80*, 171–176.

de Bergh, C., V. I. Moroz, F. W. Taylor, D. Crisp, B. Bézard, and L. V. Zasova (2006), The composition of the atmosphere of Venus below 100 km altitude: An overview, *Planet. Space Sci.*, *54*, 1389–1397.

Fedorova, A., et al. (2008), HDO and H_2O vertical distributions and isotopic ratio in the Venus mesosphere by Solar Occultation at Infrared spectrometer on board Venus Express, *J. Geophys. Res.*, *113*, E00B22, doi:10.1029/2008JE003146.

Ford, J. P., J. J. Plaut, C. M. Weitz, T. G. Farr, D. A. Senske, E. R. Stofan, G. Michaels, and T. J. Parker (1993), Guide to Magellan image interpretation, *JPL Publ.*, *93-24*.

Gupta, M. C. (2001), *Atomic and Molecular Spectroscopy*, New Age Int., New Delhi.

Harvey, A. H., and E. W. Lemmon (2005), Method for estimating the dielectric constant of natural gas mixtures, *Int. J. Thermophys.*, *26*(1), 31–46.

Harvey, A. H., and J. M. Prausnitz (1987), Dielectric constants of fluid mixtures over a wide range of temperature and density, *J. Solution Chem.*, *16*(10), 857–869.

Ho, W., I. A. Kaufman, and P. Thaddeus (1966), Laboratory measurement of microwave absorption in models of the atmosphere of Venus, *J. Geophys. Res.*, *71*(21), 5091–5108.

Howington-Kraus, E., R. Kirk, D. Galuszka, T. Hare, and B. Redding (2001), Validation of the USGS sensor model for topographic mapping of Venus using Magellan radar stereoimagery, paper presented at Extraterrestrial Mapping Workshop "Planetary Mapping 2001," U.S. Geol. Surv., Flagstaff, Ariz.

James, E. P., O. B. Toon, and G. Schubert (1997), A numerical microphysical model of the condensational Venus cloud, *Icarus*, *129*, 147–171.

Janssen, M. A., and R. L. Poynter (1981), The microwave absorption of SO_2 in the Venus atmosphere, *Icarus*, *46*, 51–57.

Jenkins, J. M., P. G. Steffes, D. P. Hinson, J. D. Twicken, and G. L. Tyler (1994), Radio occultation studies of the Venus atmosphere with the Magellan spacecraft: 2. Results from the October 1991 experiments, *Icarus*, *110*, 79–94.

Jenkins, J. M., M. A. Kolodner, B. J. Butler, S. H. Suleiman, and P. G. Steffes (2002), Microwave remote sensing of the temperature and distribution of sulfur compounds in the lower atmosphere of Venus, *Icarus*, *158*, 312–328.

Keating, G. M., et al. (1985), VIRA (Venus International Reference Atmosphere) models of Venus neutral upper atmosphere: Structure and composition, *Adv. Space Res.*, *5*(11), 117–171.

Kirkwood, J. G. (1936), On the theory of dielectric polarization, *J. Chem. Phys.*, *4*(6), 592–601.

Kirkwood, J. G. (1939), The dielectric polarization of polar liquids, *J. Chem. Phys.*, *7*, 911–919.

Knollenberg, R. G., and D. M. Hunten (1980), The microphysics of the clouds of Venus: Results of the Pioneer Venus Particle Size Spectrometer Experiment, *J. Geophys. Res.*, *85*(A13), 8039–8058.

Kolbe, W. F., H. Buscher, and B. Leskovar (1977), Microwave absorption coefficients of atmospheric pollutants and constituents, *J. Quant. Spectrosc. Radiat. Transfer.*, *18*, 47–64.

Kolodner, M. A., and P. G. Steffes (1998), The microwave absorption and abundance of sulfuric acid vapor in the Venus atmosphere based on new laboratory measurements, *Icarus*, *132*, 151–169.

Kong, J. A. (1990), *Electromagnetic Wave Theory*, John Wiley, Hoboken, N. J.

Kuczkowski, R. L., R. D. Suenram, and F. J. Lovas (1981), Microwave spectrum, structure, and dipole moment of sulfuric acid, *J. Am. Chem. Soc.*, *103*, 2561–2566.

Lide, D. R. (Ed.) (2000), *Handbook of Chemistry and Physics*, 81st ed., CRC Press, Boca Raton, Fla.

Marcq, E., B. Bézard, P. Drossart, G. Piccioni, J. M. Reess, and F. Henry (2008), A latitudinal survey of CO, OCS, H_2O, and SO_2 in the lower atmosphere of Venus: Spectroscopic studies using VIRTIS-H, *J. Geophys. Res.*, *113*, E00B07, doi:10.1029/2008JE003074.

Moroz, V. I., and L. V. Zasova (1997), VIRA-2: A review of inputs for updating the Venus International Reference Atmosphere, *Adv. Space Res.*, *19*(8), 1191–1201.

Pätzold, M., et al. (2007), The structure of Venus's middle atmosphere and ionosphere, *Nature*, *450*(429), 657–660.

Pettengill, G. H., P. G. Ford, and R. A. Simpson (1996), Electrical properties of the Venus surface from bistatic radar observations, *Science*, *272*, 1628–1631.

Phillips, R. J., and N. R. Izenberg (1995), Ejecta correlations with spatial crater density and Venus resurfacing history, *Geophys. Res. Lett.*, *22*, 1617–1620.

Phillips, R. J., R. F. Raubertas, R. E. Arvidson, I. C. Sarkar, R. R. Herrick, N. Izenberg, and R. E. Grimm (1992), Impact craters and Venus resurfacing history, *J. Geophys. Res.*, *97*, 15,923–15,948.

Pitzer, K. S. (1983), Dielectric constant of water at very high temperature and pressure, *Proc. Natl. Acad. Sci. U. S. A.*, *80*, 4575–4576.

Poynter, R. L., and H. M. Pickett (1985), Submillimeter, millimeter, and microwave spectral line catalog, *Appl. Opt.*, *24*(14), 2235–2240.

Seiff, A., J. T. Schofield, A. J. Kliore, F. W. Taylor, S. S. Limaye, H. E. Revercomb, L. A. Sromovsky, V. V. Kerzhanovich, V. I. Moroz, and M. Y. Marov (1985), Models of the structure of the atmosphere of Venus from the surface to 100 kilometers altitude, *Adv. Space Sci.*, *5*(11), 3–58.

Steffes, P. G. (1985), Laboratory measurements of the microwave opacity and vapor pressure of sulfuric acid vapor under simulated conditions for the middle atmosphere of Venus, *Icarus*, *64*, 576–585.

Steffes, P. G., and V. R. Eshleman (1981a), Sulfur dioxide and other cloud-related gases as the source of the microwave opacity of the middle atmosphere of Venus, *Icarus*, *46*, 127–131.

Steffes, P. G., and V. R. Eshleman (1981b), Laboratory measurements of the microwave opacity of sulfur dioxide and other cloud-related gases under simulated conditions for the middle atmosphere of Venus, *Icarus*, *48*, 180–187.

Stratton, A. J. (1968), Optical and radio refraction on Venus, *J. Atmos. Sci.*, *25*, 666–667.

Suleiman, S. H., M. A. Kolodner, and P. G. Steffes (1996), Laboratory measurement of the temperature dependence of gaseous sulfur dioxide (SO_2) microwave absorption with application to the Venus atmosphere, *J. Geophys. Res.*, *101*(E2), 4623–4635.

Svedhem, H., et al. (2007), Venus Express—The first European mission to Venus, *Planet. Space Sci.*, *55*, 1636–1652.

Tellmann, S., M. Päzold, B. Haeusler, M. K. Bird, and G. L. Tyler (2009), Structure of the Venus neutral atmosphere as observed by the Radio Science experiment VeRa on Venus Express, *J. Geophys. Res.*, *114*, E00B36, doi:10.1029/2008JE003204.

Uematsu, M., and E. U. Franck (1980), Static dielectric constant of water and steam, *J. Phys. Chem. Ref. Data*, *9*(4), 1291–1306.

Ulaby, F. T., R. K. Moore, and A. K. Fung (1981), *Microwave Remote Sensing: Active and Passive*, vol. 1, *Microwave Remote Sensing Fundamentals and Radiometry*, Artech House, Norwood, Mass.

Vandaele, A. C., et al. (2008), Composition of the Venus mesosphere measured by Solar Occultation at Infrared on board Venus Express, *J. Geophys. Res.*, *113*, E00B23, doi:10.1029/2008JE003140.

Zasova, L. V. (1995), The structure of the Venusian atmosphere at high latitudes, *Adv. Space Res.*, *16*(6), 89–98.

Zasova, L. V., V. I. Moroz, V. M. Linkin, I. V. Khatuntsew, and B. S. Maiorov (2006), Structure of the Venusian atmo-

sphere from surface up to 100 km, *Cosmic Res.*, *44*(4), 364–383.

X. Duan and M. Moghaddam, Department of Electrical Engineering and Computer Science, University of Michigan, 1301 Beal Ave., Ann Arbor, MI 48109-2122, USA. (xduan@umich.edu; mmoghadd@eecs.umich.edu)

R. L. Jordan, S. E. Smrekar, and D. Wenkert, Jet Propulsion Laboratory, 4800 Oak Grove Dr., Pasadena, CA 91109, USA. (rolando.l.jordan@jpl.nasa.gov; suzanne.e.smrekar@jpl.nasa.gov; daniel.wenkert@jpl.nasa.gov)